# First-Principles Study of Half-Metallic Behavior in Vanadium Nitride (VN): Structural, Electronic, and Optical Properties of Rock Salt and Zinc Blende Structures

Ammar A. Kadhim\*

Department of Chemistry, College of Education / Qurna, University of Basrah, Basrah, Iraq.

#### ARTICLE INFO

#### ABSTRACT

Received 19 April 2025 Revised 20 June 2025 Accepted 25 June 2025 Published 31 June 2025

#### Keywords:

Half-Metallic; DFT; 3D; Magnetic Moment; Optical Properties.

Citation: A. A. Kadhim, J.Basrah Res. (Sci.) **51**(1),210 (2025). DOI: <a href="https://doi.org/10.56714/b">https://doi.org/10.56714/b</a> jrs.51.1.18 The bulk optical and electrical characteristics of VN are investigated using first-principles simulations. The optimized lattice constants for rock salt and zinc blend are 6.403 Å and 7.22 Å, respectively. Both structures exhibit half-metallic behavior with metallic conductivity for spin-up electrons and semiconducting behavior for spin-down electrons. The zinc blend contains a direct band gap of 6.18 eV, whereas rock salt has a direct band gap of 3.77 eV. The total magnetic moment of both structures is 2  $\mu B$  per unit formula. In the bulk Heusler lattice, the magnetic moment value shows that the structure behaves half-metallically in both the rock-salt and zinc-blende configurations.

By calculating key optical parameters, including the dielectric function, absorption coefficient, and optical spectra within the 0-15 eV energy range, the material demonstrates significant potential for spintronic devices and optoelectronic applications.

ISSN: 1817-2695 (Print); 2411-524X (Online)

Online at: https://jou.jobrs.edu.iq

#### 1. Introduction

Meanwhile, the groundbreaking proposal of half-metallic magnets by de Groot and colleagues in 1983 has garnered significant scientific interest, particularly because of their unique electronic properties and potential applications in spintronics [1]. The rapid progress in giant magneto-resistive (GMR) technology has further driven the demand for novel materials with high spin polarization or enhanced spin-filtering capabilities [2]. The spin-up and spin-down electronic bands in half-metallic materials behave differently: the spin-up band is the Fermi energy level (Ef) and is metallic, but the spin-down band has an energy gap at Ef and is a semiconductor.

To optimize the performance of spintronic devices, it is essential to advance semi-metallic compounds that can serve as ideal spin injectors into semiconductors, ensuring fully spin-polarized currents. These materials have found diverse applications in spintronics, including non-volatile random-access memories, magnetic tunnel junctions, magnetic sensors, spin injectors, spin light-emitting diodes, and field-effect transistors, among others [3, 4, 5, 6, 7, 8, 9, 10]. The discovery of half-metallic magnets

\*Corresponding author email: ammar.kadhim@uobasrah.edu.iq



has expanded the scope of spintronics and spurred extensive research into their properties and potential uses. Concerning nonvolatility, larger transistor density, and faster data processing, spintronic systems perform better than conventional electrical devices [11].

The half-metallic ferromagnet status of Ca pnictides with zinc flint structures containing CaP, CaAs, and CaSb was proposed by Geshi et al. [12] in 2004. In the absence of transition metal atoms in three-dimensional magnetic compounds, half-metallic ferromagnetism differs from double or p—d exchange mechanisms. As a result, these materials are classified as sp half-metallic ferromagnets. Subsequently, numerous research groups have conducted comprehensive studies on I–V and II-IV zinc blende compounds [8, 13, 14, 15].

Detailed descriptions of MC (M = Ca, Sr, Ba) compounds with zincblende and rock-salt structures [16, 17] suggest that they exhibit half-metallic ferromagnetism above room temperature for zincblende CaC, SrC, and rock-salt SrC, BaC. Furthermore, Zhang and Gao predicted that MX with a zinc-blende structure (M = Li, Na, K, X = C, S) would be half-metallic ferromagnetic [18, 19]. Unfortunately, half-metallic ferromagnetism is almost always present in MC (M = Li, Na, K) with rock salt structure, indicating that the half-metallic gap does not exist.

In this study, density functional theory (DFT) is applied to explore three-dimensional VN electronic and optical properties. The primary focus is to analyze the electronic band structure and optical properties of bulk VN in both rock- salt and zinc- blende structures.

#### 2. Computational methods

VN alloys' structural, magnetic, electrical, and optical properties were thoroughly investigated using the CASTEP code in density functional theory (DFT) computations [20]. The Perdew-Burke-Ernzerhof (PBE) functional inside the generalized gradient approximation (GGA) was used to describe the exchange and correlation energies to guarantee the accuracy of the band structure computations [21]. A  $15 \times 15 \times 15$  k-point Monkhorst-Pack grid was used for the Brillouin zone integration in reciprocal space. The muffin-tin sphere radius (Rmt) of both vanadium (V) and nitrogen (N) atoms was set to 2.5 atomic units (a.u.). Structural relaxation was achieved by converging the interatomic forces to less than 0.01 eV/Å, and a total energy convergence criterion of  $10^{-15}$  eV and a plane wave cutoff energy of 400 eV were applied. These carefully selected computational parameters ensured a reliable and detailed analysis of the structural, electrical, and optical properties of VN alloys.

## 3. The results and discussion

#### 3.1. The structural and electronic properties

Rocksalt and zinc blende (ZB) have unique crystal structures. As shown in Figure 1, rocksalt VN belongs to the space group FM-3M (No. 225), with V and N atoms at locations (0,0,0) and (0.5,0.5,0.5), respectively. In contrast, ZB VN belongs to the space group F43M (No. 216), with atomic coordinates for V at (0, 0, 0) and N at (0.25, 0.25, 0.25).

When the bulk electronic characteristics of VN are analyzed using the Heusler alloy model, several electrical defects are discovered. The direct band gap between the large valence band and the low conduction band refers to metallic behavior in the spin-minority channel. However, semiconducting properties are added by the Fermi band crossover for the spin-majority channel. Figure 2 illustrates one example of this kind of behavior. According to these observations, both the ZB and rock-salt structures of VN display half-metallic ferromagnetic properties. The bulk rock-salt (RS) VN structure displays a direct bandgap of 3.77 eV, while the bulk zincblende (ZB) structure exhibits a notably larger direct bandgap of 6.18 eV. A detailed analysis of the half-metal gap (HM gap) found that the minimum energy difference between the Fermi level and the valence band maximum or conduction band minimum is referred to as the half-metal gap (HM gap).

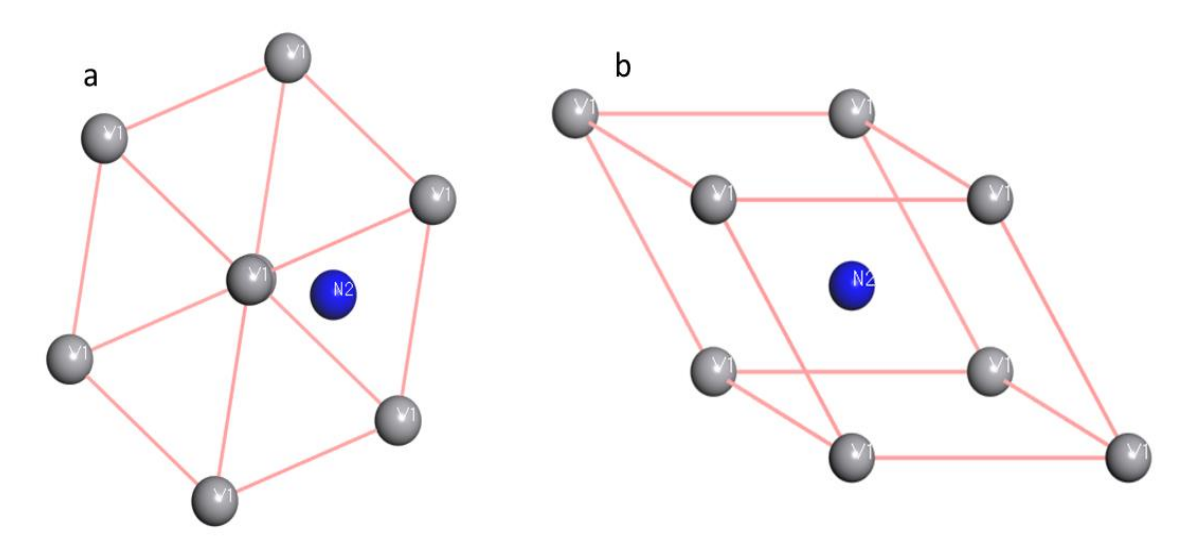
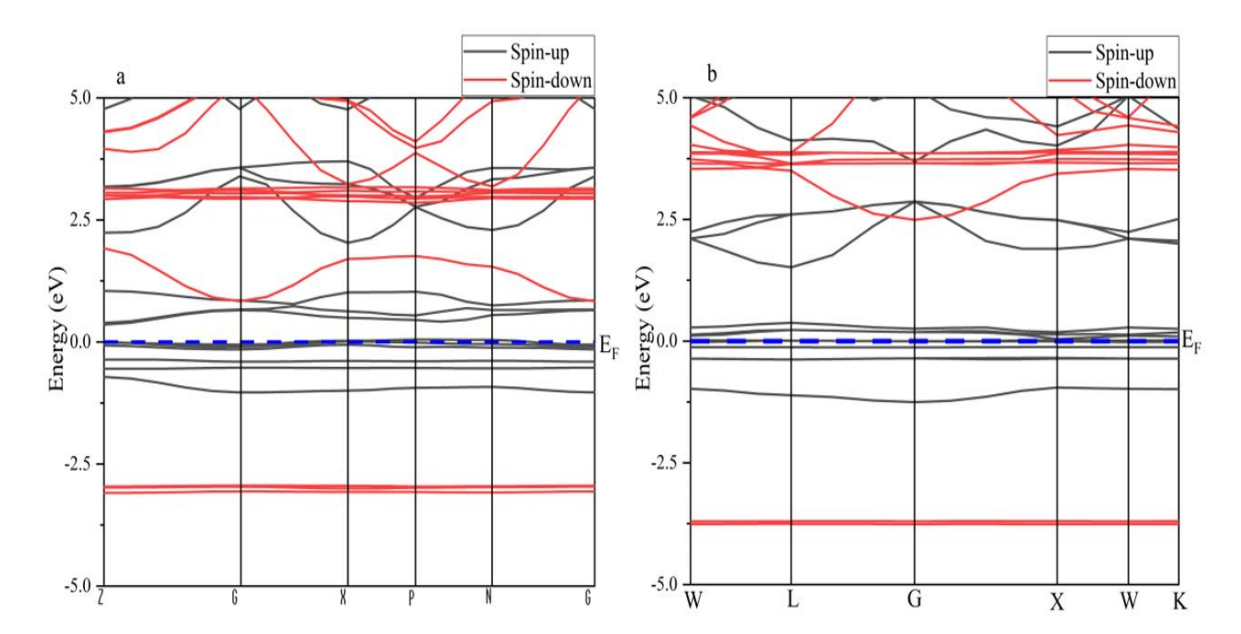


Fig. 1. VN crystal structures with (a) rocksalt phases and (b) zinc-blende.



**Fig. 2.** depicts the spin-polarized band structures of (a) rocksalt and (b) zincblende. At the anticipated equilibrium lattice constant.

## 3.2. Magnetic characteristics and density of states

Figures 3(a, b) and 4(a, b)

shows that the partial and total density of states of VN half-Heusler alloys were analyzed in detail at equilibrium lattice constants. The Fermi energy level was set at 0 eV, and the low spin states were inverted by multiplying by -1. The clear peak observed in the valence region at -1.2 eV is mainly due to the contribution of vanadium (V) atoms, with minimal contribution from nitrogen (N) atoms. In the minority spin DOS, the N states dominate the valence band and the V states dominate the conduction band, suggesting the existence of a band gap [22]. In contrast, the majority spin DOS shows a peak at the Fermi energy (EF) level, indicating metallic behavior with majority spin channels. Furthermore, the effect of the change in lattice constant on the energy gap is briefly discussed. In VN, the band gap arises from the hybridization d orbitals of V and the p orbitals of N. This interaction within the bulk structures preserves the inherent half-metallic (HM) characteristics of VN, with the primary source of

its magnetic properties attributed to the large spin magnetic moment of the V atom [23]. As shown in Figures 3(b) and 4(b), this behavior stems from the higher electron occupation in the outer d shell of the vanadium (V) atom relative to the other constituent atoms. According to the Slater–Pauling rule [22, 23], the VN alloy has 10 valence electrons total, which are contributed by the valence electron configurations of V (4d³ 4s²) and N (2s² 2p³). The formula of the rule is Mt = Zt - 8, where Zt is the total number of valence electrons of the atomic cell. This leads to a total magnetic moment of 2  $\mu$ B. Nitrogen atoms contribute a rather small amount of the total magnetic moment, but the Vanadium atoms have a greater magnetic moment compared with the Nitrogen atom, creation for the majority.

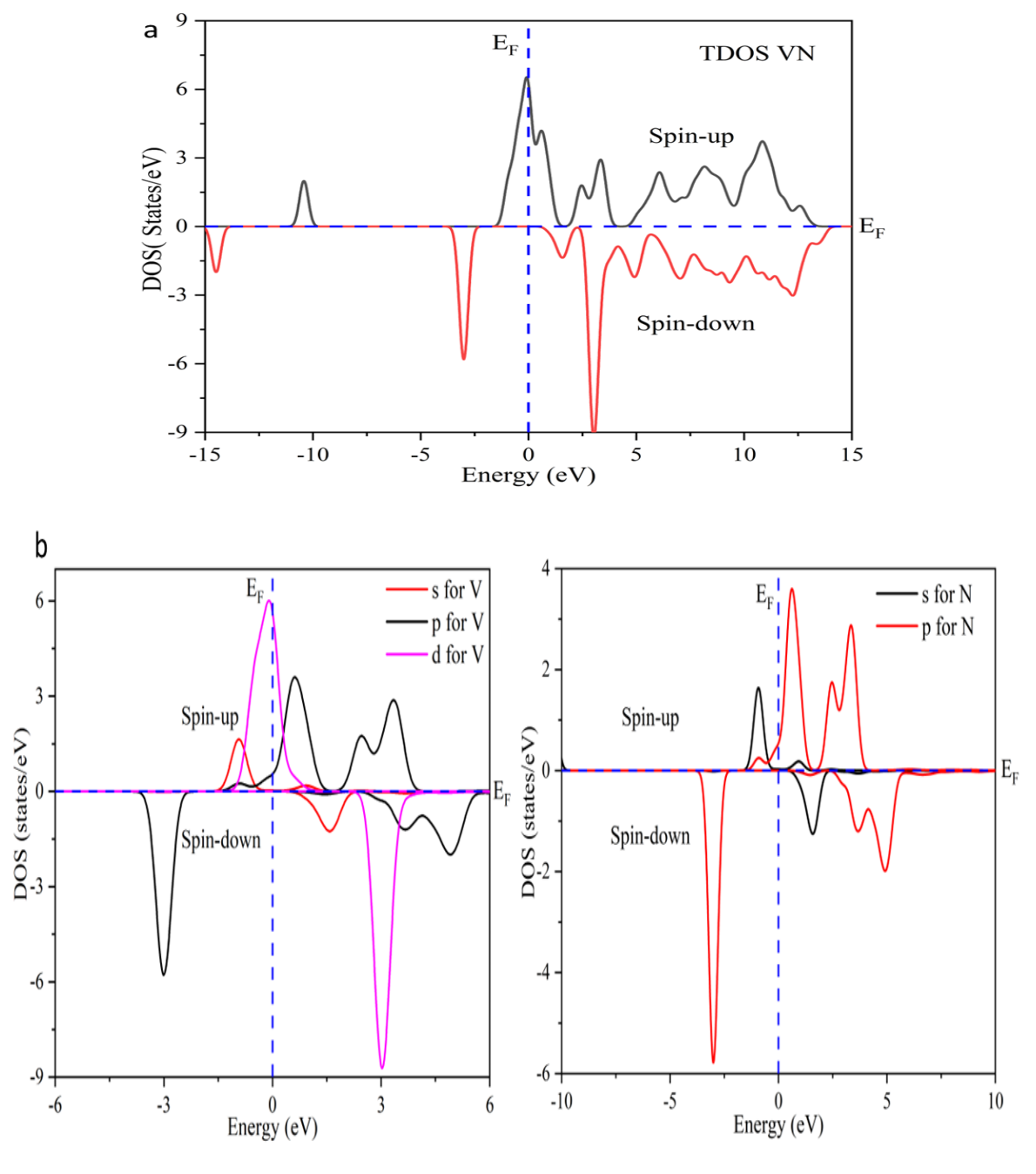


**Fig. 3.** (a) Total density of states (TDOS) for the VN rock salt. (b) Partial density of states (PDOS) for V and N orbitals in the VN rock salt.

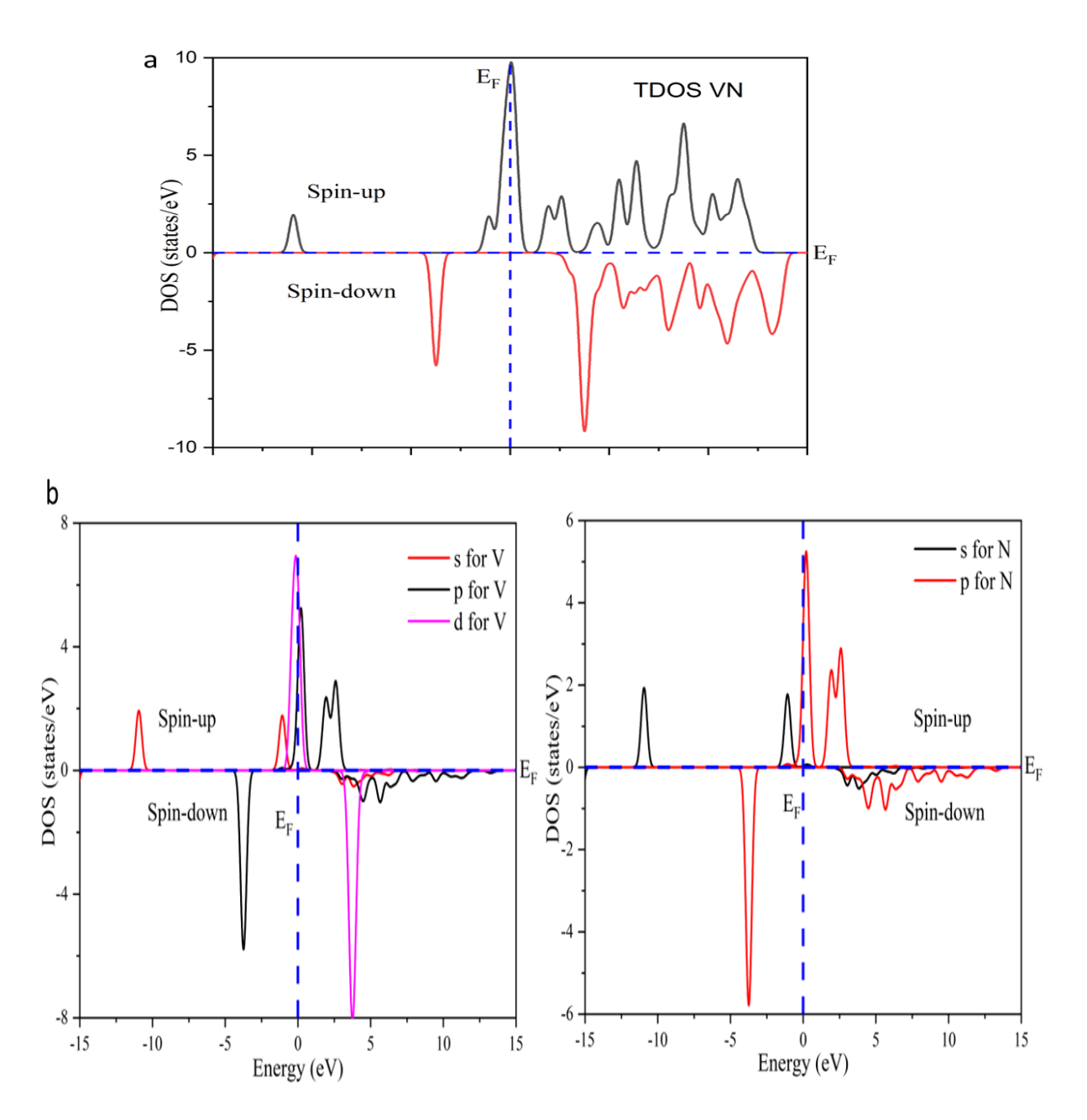


**Fig. 4.** (a) The total density of states (TDOS) for bulk zinc blend VN. (b) V and N orbitals partial density of states (PDOS) in bulk zinc-blend VN.

## 3.3. Optical properties

Figure 5 shows the energy dependence of the bulk VN optical spectrum. This study focuses on the energy ranges of 0–50 eV for Absorbance and 0–15 eV for the dielectric function to comprehensively analyze the compound's optical properties for practical applications. The Tran-Blaha-modified Becke-Johnson (TB-mBJ) method, known for its accuracy in determining optical properties, was employed with a  $30\times30\times30$  k-point grid. The full-potential linear augmented plane wave (FP-LAPW) method, which uses fine-scale lattice constants and incorporates exchange and correlation effects, is used to calculate the complex dielectric function. This section presents the grades of the dielectric function  $\epsilon(\omega)$  and the Absorbance coefficient  $A(\omega)$ , where the dielectric function is defined via equation (1):

$$\varepsilon(\omega) = \varepsilon I(\omega) + i\varepsilon 2(\omega) \tag{1}$$

$$n(\omega) = \left[\frac{\sqrt{\varepsilon_1^2(\omega) + \varepsilon_2^2(\omega) + \varepsilon_1(\omega)}}{2}\right]^{1/2}$$

$$k(\omega) = \left[\frac{\sqrt{\varepsilon_1^2(\omega) + \varepsilon_2^2(\omega) - \varepsilon_1(\omega)}}{2}\right]^{1/2}$$
(3)

$$k(\omega) = \left[\frac{\sqrt{\varepsilon_1^2(\omega) + \varepsilon_2^2(\omega) - \varepsilon_1(\omega)}}{2}\right]^{1/2}$$
(3)

Figure 5(b) demonstrates the photon energy-dependent dielectric function  $\varepsilon(\omega)$ . The dielectric function is contingent on both intraband and interband transitions. Interband transitions are considered for both direct and indirect transitions, but electronic excitations through the indirect band gap are not included in the calculation. This exclusion is expressed by the fact that indirect transitions have smaller photon momenta than direct interband transitions.

Momentum matrix elements are cast off to determine the electronic band structure and the transitions between occupied and unoccupied states, which administer the dielectric function. The dielectric function's real part,  $\epsilon_1(\omega)$ , which is derived from the Kramers-Kronig relation, describes how electromagnetic waves move through the material [24]. The absorption is represented by the imaginary part,  $\epsilon_2(\omega)$ , which is computed by adding up the transitions from occupied to unoccupied states using Fermi's golden rule [25]. Figure 5(b) schematically shows the dielectric function of VN alloys, both the real and imaginary parts, as a function of photon energy in the 0-15 eV range. The dielectric constant at zero frequency is determined to be 10 for rock salt (RS) VN and 2.26 for zinc alloy (ZB)

The value of  $\varepsilon_1(0)$  shows high stability. The real part of the dielectric constant of VN remains approximately constant up to 15 eV, with negative values indicating that the incoming radiation is reflected from the surface [26]. The imaginary part of the dielectric function,  $\varepsilon_2(\omega)$ , at zero frequency, represents the optical band gap of the compound. The absorption coefficient  $A(\omega)$  is calculated to analyze the optical properties. In the low-energy range (0.0 eV), VN exhibits a slight absorption coefficient due to photon energies being below the bandgap of both rock-salt (RS) and zincblende (ZB) structures, indicating the absence of electronic transitions, as shown in Figure 5(a). However, absorption features become prominent at approximately 5 eV, as illustrated in Figure 5(a). The maximum absorption coefficients for RS VN and ZB VN are 165,000 and 140,000, respectively, occurring at 37 eV. These results demonstrate that VN, as a wide-bandgap material, possesses strong UV absorption properties, creation it appropriate for optoelectronic applications like UV detectors[27].

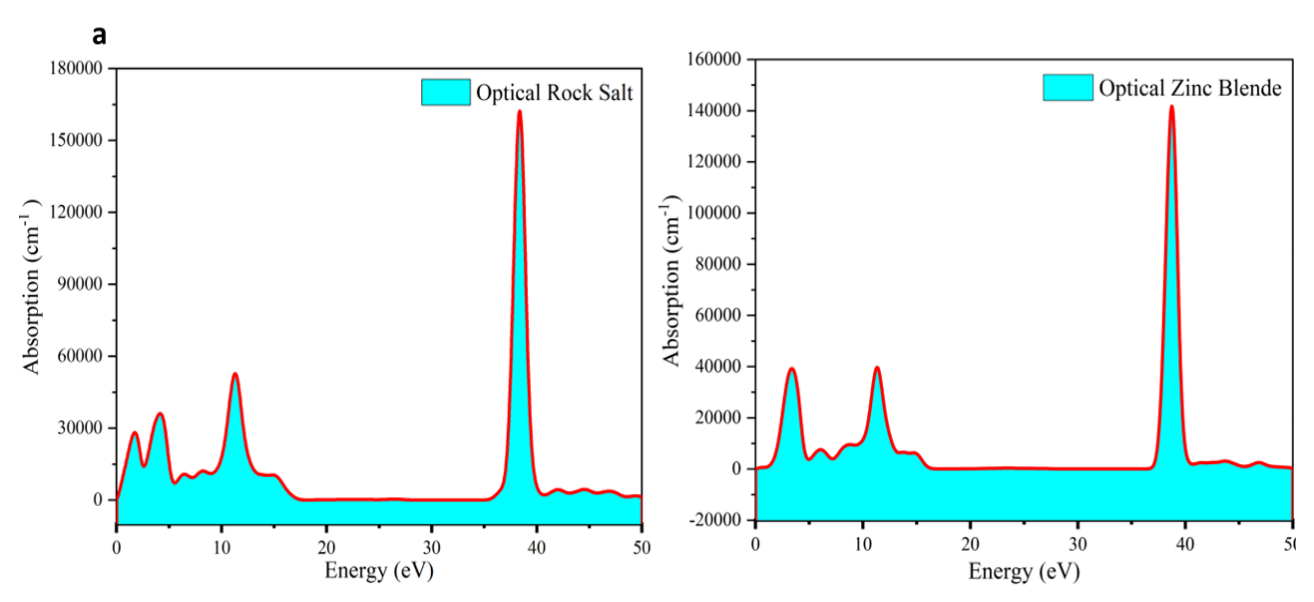


Figure 5. depicts VN properties in both bulk rock salt and zinc mix forms. Panels (a) exhibit the absorption coefficient, whereas panels (b) display both the real and imaginary components of the compound dielectric function.

#### 4. Conclusion

To summarize, we explored the optical, electrical, and structural aspects of VN. The space group of the rock salt VN is FM-3M (No. 225), with V and N at (0, 0, 0) and (0.5, 0.5, 0.5), respectively; the ZB VN has atomic coordinates V at (0, 0, 0) and N at (0.25, 0.25, 0.25) and belongs to space group F-43M (No. 216). The ZB equilibrium lattice constant is 6.18 Å, while the bulk rock salt is 3.77 Å. The inferred band structure is shown to have substantial half-metallic properties in common with VN alloys. A total magnetic moment is  $2 \mu B$ , portentous that a Slater-Polling rule (Mt = Zt-8) was used.

## References

- [1] X.-P. Wei, W. Sun, Y.-L. Zhang, X.-W. Sun, T. Song, T. Wang, J.-L. Zhang, H. Su, J.-B. Deng, and X.-F. Zhu, "Investigations on electronic, Fermi surface, Curie temperature and optical properties of Zr2CoAl," *Journal of Solid State Chemistry*, vol. 247 ,pp. 97-104, 2017. DOI: https://doi.org/10.1016/j.jssc.2017.01.002.
- [2] Z. Wang, H. Wang, L. Wang, H. Zhao, M. A. Kamboh, L. Hao, Q. Chen, K. He, and Q. Wang, "Influence of Cu dopant on the electronic and optical properties of graphene-like ZnO monolayer," *Physica E: Low-Dimensional Systems and Nanostructures*, vol. 115, pp. 113702, 2020. DOI:https://doi.org/10.1016/j.physe.2019.113702.
- [3] J. Coey, "d0 ferromagnetism," *Solid state sciences*, vol. 7, no. 6, pp. 660-667, 2005. DOI:https://doi.org/10.1016/j.solidstatesciences.2004.11.012.
- [4] J. Beltrán, C. Monty, L. Balcells, and C. Martínez-Boubeta, "Possible d0 ferromagnetism in MgO," *Solid State Communications*, vol. 149, no. 39-40, pp. 1654-1657, 2009. DOI:https://doi.org/10.1016/j.ssc.2009.06.044.
- [5] W. Adli, and M. Ferhat, "d0 Ferromagnetism in oxygen-doped CuCl: First principles study," *Solid state communications*, vol. 189, pp. 68-71, 2014. DOI:https://doi.org/10.1016/j.ssc.2014.03.013.
- [6] J. Du, S. Dong, Y.-L. Lu, H. Zhao, L. Feng, and L. Wang, "Half-metallic ferromagnetic features in d0 quaternary-Heusler compounds KCaCF and KCaCCl: A first-principles description," *Journal of Magnetism and Magnetic Materials*, vol. 428, pp. 250-254, 2017. DOI:https://doi.org/10.1016/j.jmmm.2016.12.038.
- [7] M. Kazemi, P. Amiri, and H. Salehi, "Density functional study of d0 half-metallic ferromagnetism in a bulk and (001) nano-surface of KP compound," *Physics Letters A*, vol. 381, no. 30, pp. 2420-2425, 2017. DOI: https://doi.org/10.1016/j.physleta.2017.05.027.
- [8] G. Gao, K. Yao, Z. Liu, J. Zhang, Y. Min, and S. Fan, "A first-principles study of half-metallic ferromagnetism in binary alkaline-earth nitrides with rock-salt structure," *Physics letters A*, vol. 372, no. 9, pp. 1512-1515, 2008. DOI:https://doi.org/10.1016/j.physleta.2007.09.064.
- [9] R. A. De Groot, F. M. Mueller, P. v. van Engen, and K. Buschow, "New class of materials: half-metallic ferromagnets," *Physical review letters*, vol. 50, no. 25, pp. 2024, 1983. DOI:https://doi.org/10.1103/PhysRevLett.50.2024?\_gl=1\*1i4rqom\*\_ga\*ODk1Mjk4OTYzLjE3N DE5NDg1NzQ.\*\_ga\_ZS5V2B2DR1\*MTc0MTk0ODU3NC4xLjAuMTc0MTk0ODU3NC4wLj AuMzk2MjA0NTk1.
- [10] S. Wolf, D. Awschalom, R. Buhrman, J. Daughton, v. S. von Molnár, M. Roukes, A. Y. Chtchelkanova, and D. Treger, "Spintronics: a spin-based electronics vision for the future," *science*, vol. 294, no ,5546 .pp. 1488-1495, 2001. DOI:https://doi.org/10.1126/science.1065389.
- [11] H. Ohno, "Making nonmagnetic semiconductors ferromagnetic," *science*, vol. 281, no. 5379, pp. 951-956, 1998. DOI:https://doi.org/10.1126/science.281.5379.951.
- [12] K. Kusakabe, M. Geshi, H. Tsukamoto, and N. Suzuki, "New half-metallic materials with an alkaline earth element," *Journal of Physics: Condensed Matter*, vol. 16, no. 48, pp. S5639, 2004. DOI:https://doi.org/10.1088/0953-8984/16/48/021.
- [13] M. Sieberer, J. Redinger, S. Khmelevskyi, and P. Mohn, "Ferromagnetism in tetrahedrally coordinated compounds of I/II-V elements: Ab initio calculations," *Physical Review B—Condensed Matter and Materials Physics*, vol. 73, no. 2, pp. 024404, 2006. DOI: DOI:https://doi.org/10.1103/PhysRevB.73.024404

- [14] G. Gao, K. Yao, E. Şaşıoğlu, L. Sandratskii, Z. Liu, and J. Jiang, "Half-metallic ferromagnetism in zinc-blende CaC, SrC, and BaC from first principles," *Physical Review B—Condensed Matter and Materials Physics*, vol. 75, no. 17, pp. 174442, 2007. DOI: DOI:https://doi.org/10.1103/PhysRevB.75.174442
- [15] G. Gao, and K. Yao, "Half-metallic sp-electron ferromagnets in rocksalt structure: The case of SrC and BaC," *Applied physics letters*, vol. 91, no. 8, 2007. DOI:https://doi.org/10.1063/1.2775081.
- [16] R. R. Palanichamy ,G. S. Priyanga, A. J. Cinthia, A. Murugan, A. A. Meenaatci, and K. Iyakutti, "Half metallic ferromagnetism in alkaline-earth metal nitrides XN (X= Ca, Sr and Ba): A first principles study," *Journal of magnetism and magnetic materials*, vol. 346, pp. 26-3.2013 ,7. DOI:https://doi.org/10.1063/1.3586257.
- [17] A. A. Kadhim, H. Sedghi, and J. M. K. Al-zyadi, "Investigation of structural, electronic, and optical properties of bulk and monolayer for new material CrS under electric field effect," *Journal of Magnetism and Magnetic Materials*, vol. 603 ,pp. 172276, 2024. DOI:https://doi.org/10.1016/j.jmmm.2024.172276.
- [18] C.-W. Zhang, "Half-metallic ferromagnetism in the zinc-blende MC (M= Li, Na and K)," *Journal of Physics D: Applied Physics*, vol. 41, no. 8, pp. 085006, 2008. DOI:https://doi.org/10.1088/0022-3727/41/8/085006.
- [19] G. Gao, K. Yao, M. Song, and Z. Liu, "Half-metallic ferromagnetism in rocksalt and zinc-blende MS (M= Li, Na and K): a first-principles study," *Journal of magnetism and magnetic materials*, vol. 323, no. 21, pp. 2652-2657, 2011. DOI:https://doi.org/10.1016/j.jmmm.2011.06.003.
- [20] S. J. Clark, M. D. Segall, C. J. Pickard, P. J. Hasnip, M. I. Probert, K. Refson, and M. C. Payne, "First principles methods using CASTEP," *Zeitschrift für kristallographie-crystalline materials*, vol. 220, no. 5-6, pp. 567-570, 2005. DOI:https://doi.org/10.1524/zkri.220.5.567.65075.
- [21] J. P. Perdew, K. Burke, and M. Ernzerhof, "Generalized gradient approximation made simple," *Physical review letters*, vol. 77, no. 18, pp. 3865, 1996. DOI: DOI:https://doi.org/10.1103/PhysRevLett.77.3865
- [22] J. C. Slater, "The ferromagnetism of nickel. II. Temperature effects," *Physical Review*, vol. 49, no. 12, pp. 931, 1936. DOI:https://doi.org/10.1103/PhysRev.49.931
- [23] L. Pauling, "The nature of the interatomic forces in metals," *Physical Review*, vol ,54 .no. 11, pp. 899, 1938. DOI: https://doi.org/10.1103/PhysRev.54.899
- [24] M. Gajdoš, K. Hummer, G. Kresse, J. Furthmüller, and F. Bechstedt, "Linear optical properties in the projector-augmented wave methodology," Physical Review B—Condensed Matter and Materials Physics, vol. 73, no. 4, pp. 045112, 2006. DOI: DOI:https://doi.org/10.1103/PhysRevB.73.045112
- [25] G. Guo, K. Chu, D.-s. Wang, and C.-g. Duan, "Linear and nonlinear optical properties of carbon nanotubes from first-principles calculations," *Physical Review B*, vol. 69, no. 20, pp. 205416, 2004. DOI: https://doi.org/10.1103/PhysRevB.69.205416
- [26] R. Saleh, and J. AL-Zyadi, "50 (1), 12",(2024) 5*DOI: https://doi. org/10.56714/bjrs*, vol. 50, no. 1.11, pp. 2, 2024. DOI:https://doi.org/10.56714/bjrs.50.1.11.
- [27] A. A. Kadhim, J. M. K. Al-zyadi, and H. Sedghi, "Investigating the electronic, optical, and elastic properties of bulk and monolayer CrAs under an electric field effect ",*Physics Letters A*, pp. 130306, 2025. DOI: https://doi.org/10.1016/j.physleta.2025.130306.

## دراسة المبادئ الأساسية للسلوك نصف المعدني في نيتريد الفاناديوم: الخصائص الهيكلية والإلكترونية والبصرية لتركيب ملح الصخور والزنك بليند

### عمار عبد الجبار كاظم \*

قسم الكيمياء، كلية التربية / القرنة، جامعة البصرة، البصرة، العراق.

#### الملخص

### معلومات البحث

تمت دراسة الخصائص الضوئية والكهربائية الأساسية لـ VN باستخدام محاكاة المبادئ الأولى. تم تحسين ثوابت الشبكة لملح الصخور والزنك بليند لتكون  $^{\rm A}$  6.403 و  $^{\rm A}$  2.20 على التوالي. يظهر كلا الهيكلين سلوكًا نصف معدني مع موصلية معدنية لإلكترونات البرم باتجاه الأعلى وسلوكًا شبه موصل لإلكترونات البرم باتجاه الأسفل. يحتوي مزج الزنك على فجوة نطاق مباشرة تبلغ 6.18 إلكترون فولت، في حين أن ملح الصخور لديه فجوة نطاق مباشرة تبلغ 3.77 إلكترون فولت. يبلغ العزم المغناطيسي الكلي لكل من الهيكلين 2  $\mu$  لكل وحدة صيغة. تشير قيمة العزم المغناطيسي إلى أن التركيب يَظهر سلوك المواد النصف معدنية في كلٍ من تركيب الملح الصخري و الزنك بلنيد، ضمن شبيكة هيوسلر الحجمية. من خلال حساب المعاملات الضوئية الرئيسية، بما في ذلك الوظيفة العازلة ومعامل الامتصاص والطيف الضوئي ضمن نطاق الطاقة من 0-15 الكترون فولت، يظهر هذا المادة إمكانيات كبيرة لأجهزة الكترونيات والتطبيقات البصرية.

الاستلام 19 نيسان 2025 المراجعة 20 حزيران 2025 القبول 25 حزيران 2025 النشر 31 حزيران 2025

## الكلمات المفتاحية

نصف معدني، DFT، ثلاثي الأبعاد، العزم المغناطيسي، الخصائص البصرية.

**Citation:** A. A. Kadhim, J.Basrah Res. (Sci.) **51**(1),210 (2025).

DOI: https://doi.org/10.56714/bjrs.51.1.18

